Supporting Information

Real-time Monitoring of Dynamic Changes in Li-Metal Deposition and Dissolution Using a MHz Impedance Sensor

Keisuke Ishikawa, Shogo Komagata*, Hiroki Kondo, and Masanori Ishigaki*

Secondary Batteries Research-Domain, Toyota Central R&D Labs., Inc., Nagakute, Aichi 4801192, Japan

Proposed sensor

Principle of the impedance measurements

Figure 1a shows a schematic diagram of the sensor circuit, where V_b denotes the battery voltage and L_b, R_b, and C_b represent the equivalent passive elements of the battery. The sensor comprises an inductor L_r, a capacitor C_r, and a switch SW_r connected in series with the battery. A resistor R_r was connected in parallel with the capacitor C_r to enable its discharge. The resonant current I_r was converted into a voltage signal V_p via a transformer composed of the inductor L_r and a pickup inductor L_p. M represents the mutual inductance between L_r and L_p, while V_{ph} is the output of the PH circuit. Battery isolation was achieved through the capacitance at the SW_r input and the transformer. When SW_r is closed at $t = 0$, the resonant current $I_r(t)$, the resonant angular frequency ω_0, and the damping factor α are given by the following expressions:

$$I_r = \frac{V_b}{L_r \omega_0} e^{-\alpha t} \sin \omega_0 t \#(S1)$$

$$\omega_0 = \sqrt{\frac{1}{L_r C_r} - \alpha^2} \#(S2)$$

$$\alpha = \frac{R_b}{2L_r} .\#(S3)$$

For Eq. $S1$ to hold, it is necessary to satisfy $\omega_0^2 > 0$. In this context, the LC resonance also incorporates C_b. Because an LIB forms an electrical double layer and exhibits an extremely large capacitance, the series impedance of C_b and C_r can be approximated as $\frac{C_b C_r}{C_b + C_r} \approx C_r$. Furthermore, by designing L_r such that $L_r \gg L_b$, the series impedance of L_b and L_r can be approximated as

$L_b + L_r \approx L_r$. Additionally, α varies according to changes in the battery resistance R_b. Thus, V_p is given by:

$$V_p(t) = \frac{MV_b\sqrt{\alpha^2 + \omega_0^2}}{L_r\omega_0} e^{-\alpha t} \sin(\omega_0 t - \beta), \#(S4)$$

$$\beta = \tan^{-1}\left(\frac{\omega_0}{\alpha}\right). \#(S5)$$

$V_p(t)$ reaches its local maximum value when $\sin(\omega_0 t + \beta) = 1$. At the local maximum, occurring at time $t_N = \frac{(4N-1)\pi + 2\beta}{2\omega_0}$ for $N = 1, 2, 3, \ldots$, Eq. S4 simplifies to:

$$V_p(t_N) = \frac{MV_b\sqrt{\alpha^2 + \omega_0^2}}{L_r\omega_0} e^{-\alpha t_N} \#(S6)$$

The voltage ratios at arbitrary times t_{N_1} and t_{N_2} ($N_1 < N_2$) are expressed as follows:

$$\frac{V_p(t_{N_1})}{V_p(t_{N_2})} = e^{\alpha(t_{N_2} - t_{N_1})}. \#(S7)$$

This equation demonstrates that the error-inducing factors, $M$and V_b, are effectively canceled. Based on Eqs. S3 and S7, R_b can be calculated as follows:

$$R_b = \frac{2L_r}{t_{N_2} - t_{N_1}} \ln \frac{\left|V_p(t_{N_1})\right|}{\left|V_p(t_{N_2})\right|}. \#(S8)$$

In a practical circuit, additional factors such as the discharge resistor R_r and parasitic resistance R_{pr} are considered, yielding the following modified expression:

$$R_b = \frac{2L_r}{t_{N_2} - t_{N_1}} \ln \frac{\left|V_p\left(t_{N_1}\right)\right|}{\left|V_p\left(t_{N_2}\right)\right|} - \frac{L_b}{C_r R_r} - R_{pr}. \#(S9)$$

It was therefore demonstrated that measurement of the peak values of $V_p(t_N)$ at any two points allows for the measurement of R_b.

Peak hold circuit

A switch-type PH circuit was used to acquire the peak voltage of the sensor. The sensitivity of the PH circuit is determined by the time constant formed by C_{ch} and R_{ch}. To capture the peak voltage during a single operation, the $C_{ch}R_{ch}$ time constant must be small. Since optimizing for a high voltage causes an overshoot at low voltage levels, and vice versa, a larger time constant was employed such that the circuit gradually tracked the peak over several cycles.

In the present application, the signal exhibited a damped oscillation, and without intervention, only the largest initial peak was observed. To address this issue, the proposed circuit incorporates a switch (SW_r) that selects the desired peak, thereby enabling capture at an arbitrary point. The PH circuit waveforms are shown in Figure S1. The switching timing of SW_s is given by $\frac{(4N-3)\pi + 2\beta}{2\omega_0}$. When the held voltage V_{ph} is below V_p, SW_{ch} is activated to charge C_{ch} until V_{ph} reaches V_p; thereafter, C_{ch} retains this voltage.

For high-frequency operations, the pulse response of the comparator and the feedback propagation delay of the circuit are critical. Figure S3a shows the minimum pulse width t_p of the comparator

output and the voltage error ΔV_{pl} that may occur when the pulse width is below this threshold. The error for the Nth pulse, $\Delta V_{pl}(N)$, is given by:

$$\Delta V_{pl}(N) = \frac{MV_b\sqrt{\alpha^2+\omega_0^2}}{L_s\omega_0}\{e^{-\alpha t_N} - e^{-\alpha\left(t_N-\frac{t_p}{2}\right)}\cos\frac{\omega_0 t_p}{2}\}.\#(S10)$$

Using the voltage ratio between two peaks, the following equation is obtained:

$$\frac{V_{ph}(N_1)}{V_{ph}(N_2)} = \frac{\frac{MV_b\sqrt{\alpha^2+\omega_0^2}}{L_s\omega_0}e^{-\alpha t_{N_1}} - \Delta V_{pl}(N_1)}{\frac{MV_b\sqrt{\alpha^2+\omega_0^2}}{L_s\omega_0}e^{-\alpha t_{N_2}} - \Delta V_{pl}(N_2)} = e^{\alpha\left(t_{N_2}-t_{N_1}\right)}.\#(S11)$$

This indicates that t_p does not affect the impedance calculation. The operational upper frequency limit is therefore determined by the pulse output limit of the comparator, $\omega_0 < \frac{\pi}{t_p}$.

Figure S3b illustrates the error ΔV_{dly} caused by the feedback delay. The rise and fall signal propagation delays are denoted as t_d, t_a is the start time for charging C_{ch}, t_w is the time elapsed from the start of charging until $V_{ph} = V_p$, V_{dd} is the supply voltage of $\mathrm{SW_{ch}}$, and V_{ph} is the voltage across C_{ch}. Consequently, the error ΔV_{dly} is given by:

$$V_{dly} = V_{ph}(t_a + t_w + t_d) - V_{ph}(t_a + t_w)$$
$$= \left(V_{dd} - V_{ph}(t_a)\right)\left(e^{-\frac{t_w}{R_{ch}C_{ch}}} - e^{-\frac{t_w+t_d}{R_{ch}C_{ch}}}\right).\#(S12)$$

This equation indicates that while a larger $C_{ch}R_{ch}$ time constant reduces the error, it also increases the convergence time, resulting in a trade-off that is similarly observed with higher target voltages.

With this in mind, the first (highest amplitude) peak was selected for measurement. According to Figure 1c, the highest peak voltage occurs at $t = 0$; however, this point is unstable because it depends on factors such as the switching speed of SW_r. In terms of the absolute value, the most stable and highest peak voltage is obtained when $\omega_0 t - \beta = \frac{\pi}{2}$. To obtain this peak, the polarity of the pick-up coil L_p was inverted, and the voltage was acquired from the inverted damped waveform.

When only the amplitude was considered, the second-highest peak was used. However, if the voltage levels are similar, the resulting ratio may result in a significant error. Optimal selection of the second peak is discussed in the following section.

Optimization

To obtain the most accurate measurement of R_b, it is crucial to select two optimal peak points from the damped oscillatory waveform. Initially, the extent to which the peak voltage $V_p(t)$ responds to changes in R_b was examined. By setting the mutual inductance M equal to L_r and differentiating Eq. S6, $\frac{\partial V_p(t)}{\partial R_b}$ can be determined as follows:

$$\frac{\partial V_p(t)}{\partial R_b} = \frac{V_b\sqrt{\alpha^2 + \omega_0^2}}{2L_r}\left(\frac{\alpha}{\omega_0^3} - \frac{t}{\omega_0}\right)e^{-\alpha t}.\#(S13)$$

In this calculation, it was assumed that $L_r = 1\,\mu\text{H}$, $C_r = 25\,\text{nF}$, and $V_b = 3.3\,\text{V}$. R_b was varied from 0.2 to 1 Ω. When R_b was small, the time at which the maximum sensitivity was observed increased.

The sensitivity was maximized when $\frac{\partial V_p(t)}{\partial R_b}$ reached an extreme value, i.e., when its time derivative of $\frac{\partial V_p(t)}{\partial R_b}$ became zero. Solving this condition leads to the optimal time t_{opt}, which is given by:

$$t_{opt} = \frac{2L_r}{R_b} + \frac{R_b}{2L_r\omega_0^2}. \#(S14)$$

Equation S14 shows that t_{opt} can be obtained based on L_r, R_b, and ω_0. Thus, after ω_0 has been determined according to the frequency characteristics of the battery, and upon setting the value of L_r, the optimal peak positions can be derived from R_b. Consequently, the two optimal PH positions are defined as follows: t_{N_1} is selected as the peak with the largest amplitude and the highest signal-to-noise ratio according to Eq. S12, while t_{N_2} is selected as the peak at which the sensitivity to resistance changes is maximized, as indicated by Eq. S14.

Subsequently, design of L_r was considered. Since, t_{opt} must correspond to the second or later peak voltage, the relationship $t_{opt} > \frac{2\pi}{\omega_0}$ must be met. By substituting this condition into Eq. S14, the lower bound of L_r can be obtained, as follows:

$$L_r > \frac{R_b}{2\omega_0}\left(\pi + \sqrt{\pi^2 - 1}\right) \#(S15)$$

Under these conditions, the choice of L_r involves a tradeoff. Specifically, a larger L_r reduces the current amplitude, as shown in Eq. S1, and allows for a smaller C_r, which reduces the power consumption. However, a larger inductance increases the parasitic resistance, leading to a greater measurement error. Conversely, if L_r is too small, the battery inductance L_b causes fluctuations in

the resonant frequency, compromising the accuracy of the battery state assessment. Therefore, it is necessary to design L_r by carefully considering these tradeoffs.

Table S1. Sensor parameters

Symbol	Description
L_r	1.1445 μH
C_r	30 nF
R_r	1 kΩ
$N_{L_r}:N_{L_p}$	4:2
C_{ch}	100 nF
R_{ch}	10 kΩ
$\frac{L_b}{C_r R_r}$	38.16 mΩ
R_{pr}	66.74 mΩ
$\Delta t(=t_{N_2}-t_{N_1})$	2.32 μs
SW_r	CSD16340Q3
SW_s	SN74AHCT1G126
SW_{ch}	SN74LVC1G126
SW_{dch}	BSS816NW
Op-amp1	AD8038
Op-amp2	AD8066

Comparator	LT1719

Table S2. Specifications of the tested commercial batteries

Model name	INR18650 M26
Sample name	NCM
Battery type	18650
Anode material	Graphite
Cathode material	$LiNi_{0.49}Co_{0.2}Mn_{0.31}O_2$
Nominal voltage	3.65 V
Cutoff voltage	2.75–4.2 V
Nominal capacity	2600 mAh
Weight	44.0 g
Standard charge current	1250 mA at 25 °C
Max charge current	2500 mA

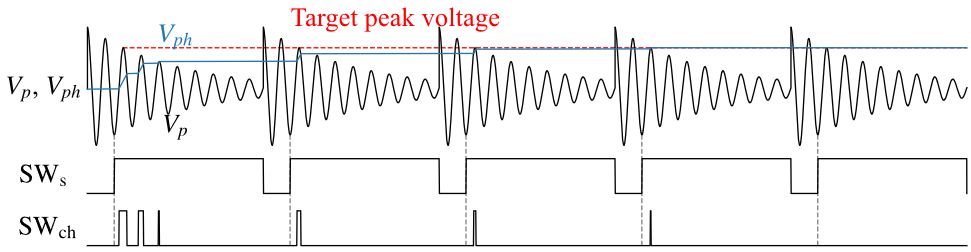

Figure S1. Operating waveforms and switch timing of the proposed PH circuit.

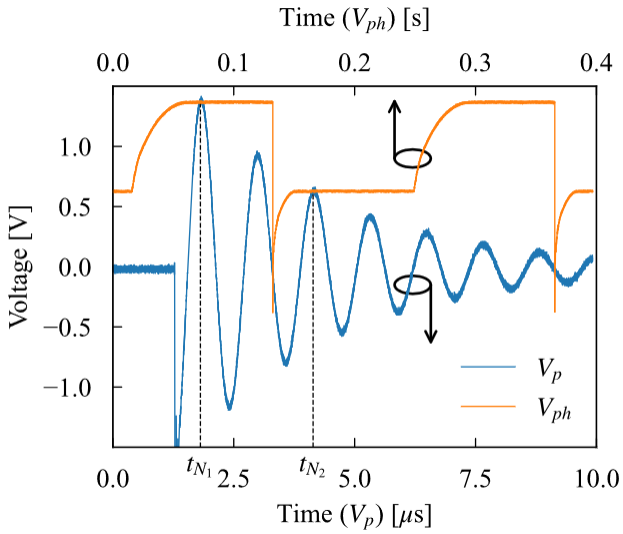

Figure S2. Experimental waveforms of the proposed PH circuit.

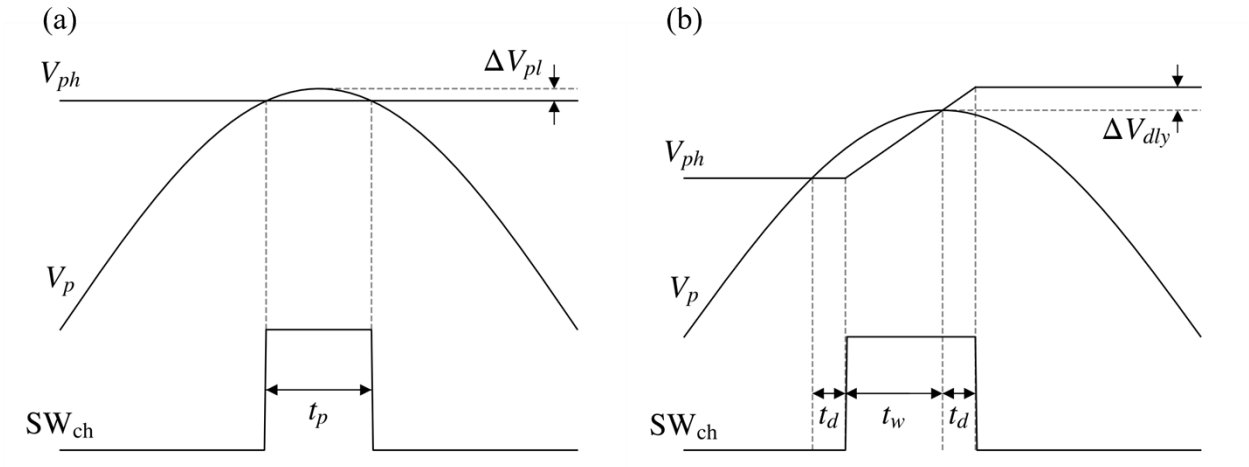

Figure S3. PH output voltage error waveforms: (a) based on the minimum pulse width and (b) based on the feedback delay.

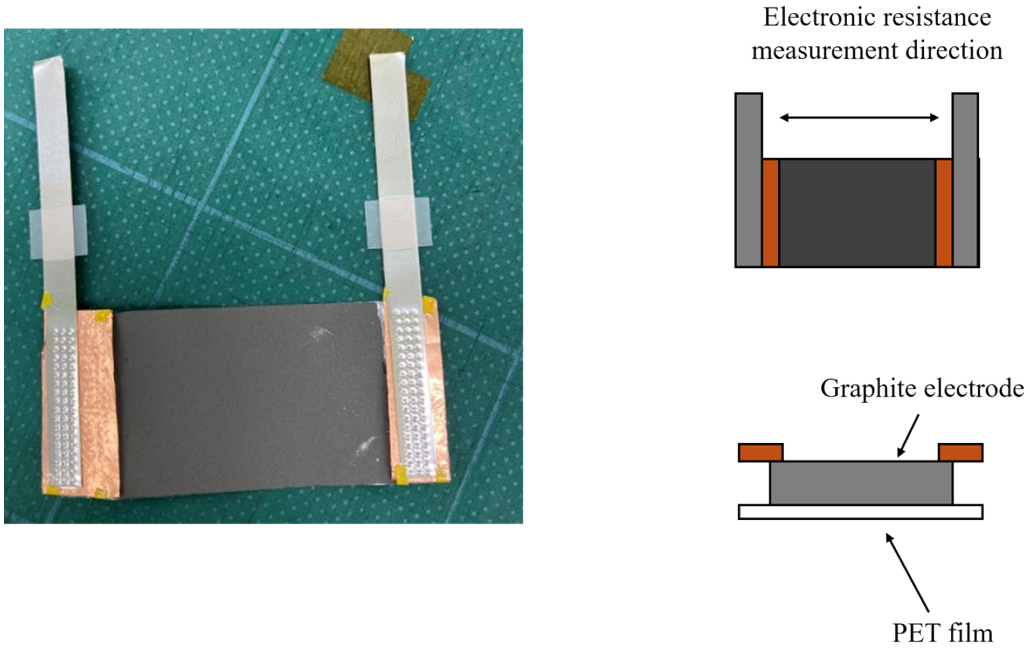

Figure S4. Photographic image and cross-sectional schematic representation of the graphite electrode used for the MHz-range Re(*Z*) measurements.

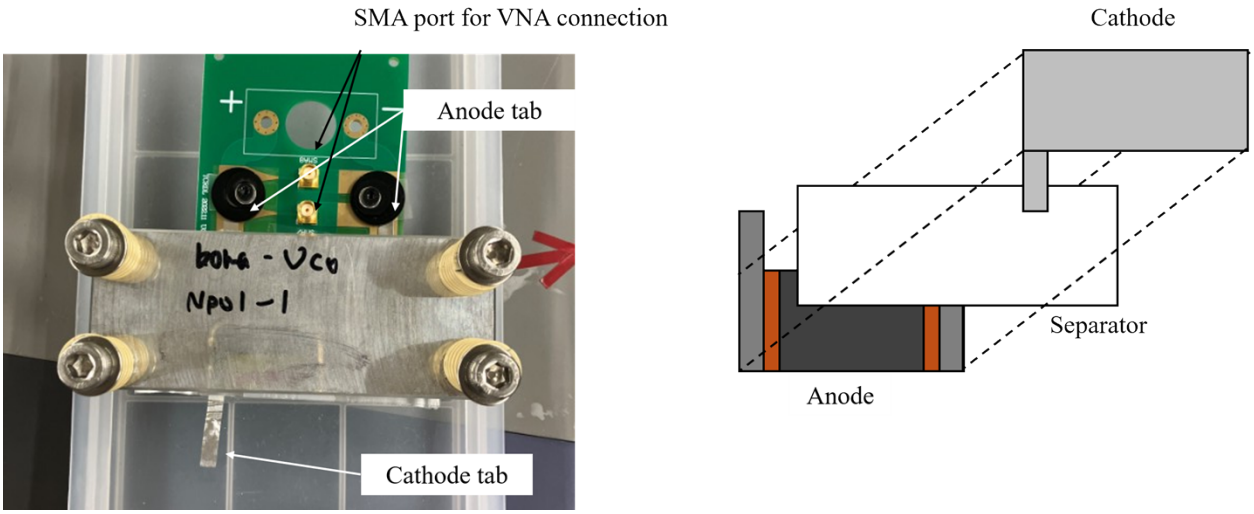

Figure S5. Cell setup used to perform the MHz-range Re(Z) measurements for the graphite electrode.

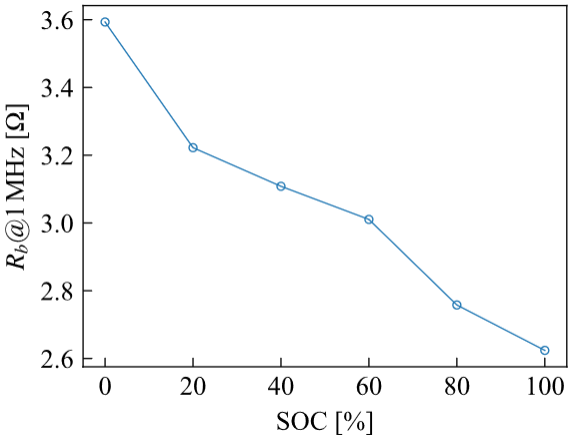

Figure S6. SOC dependence of the in-plane R_b at 1 MHz for the graphite electrode.

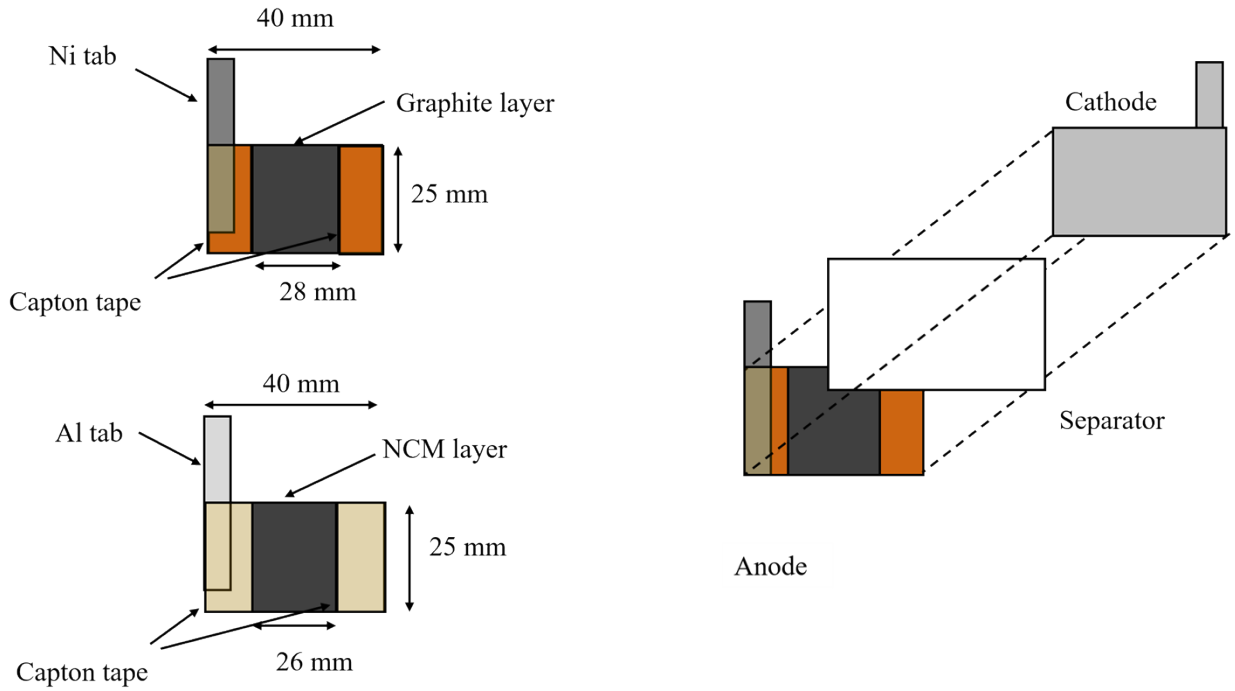

Figure S7. Schematic representation of the cross-sectional observation cell.

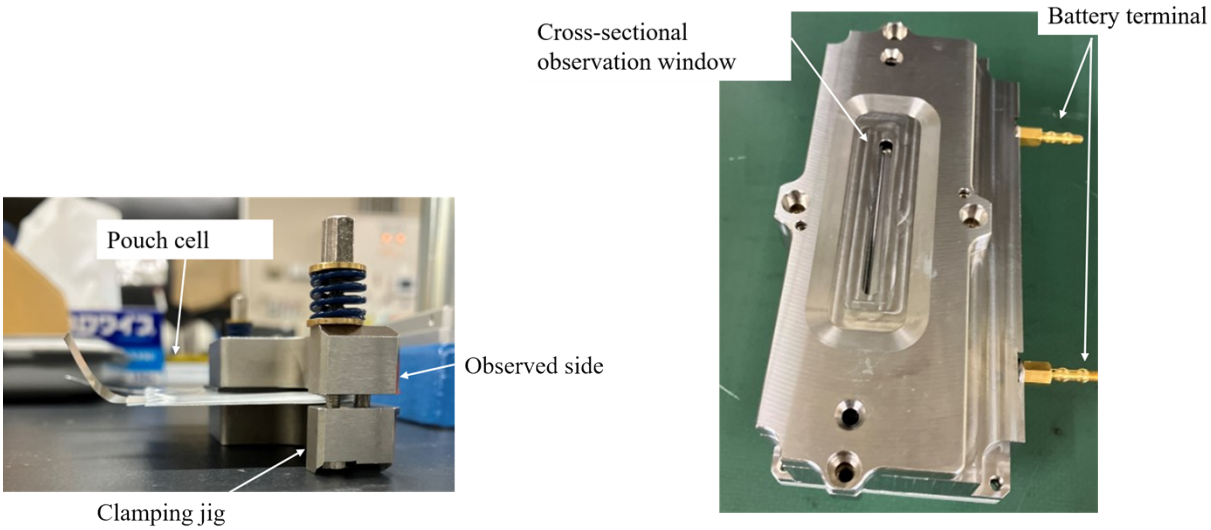

Figure S8. Photographic images of the mechanically constrained cross-sectional observation cell equipped with a viewing window.

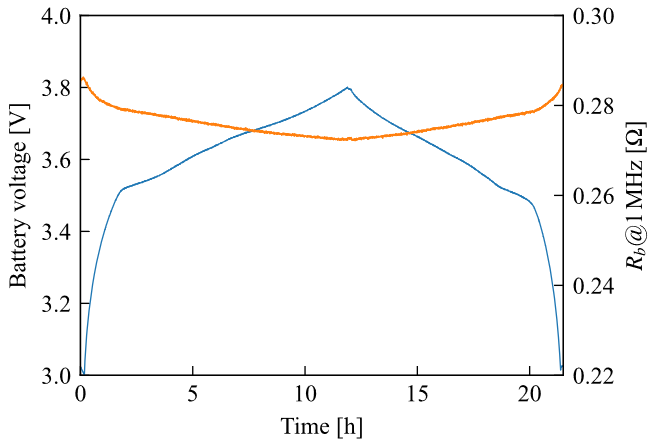

Figure S9. Battery voltage and sensor output, R_b, recorded during an charge and discharge without Li-metal deposition.

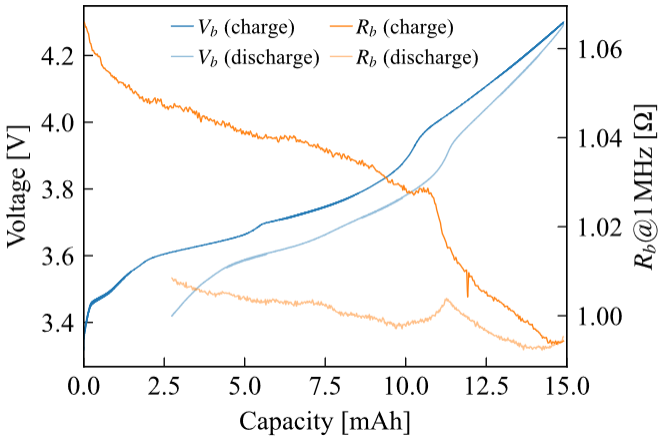

Figure S10. Plots of the battery voltage and sensor output R_b versus the delivered charge in the cross-sectional observation cell.

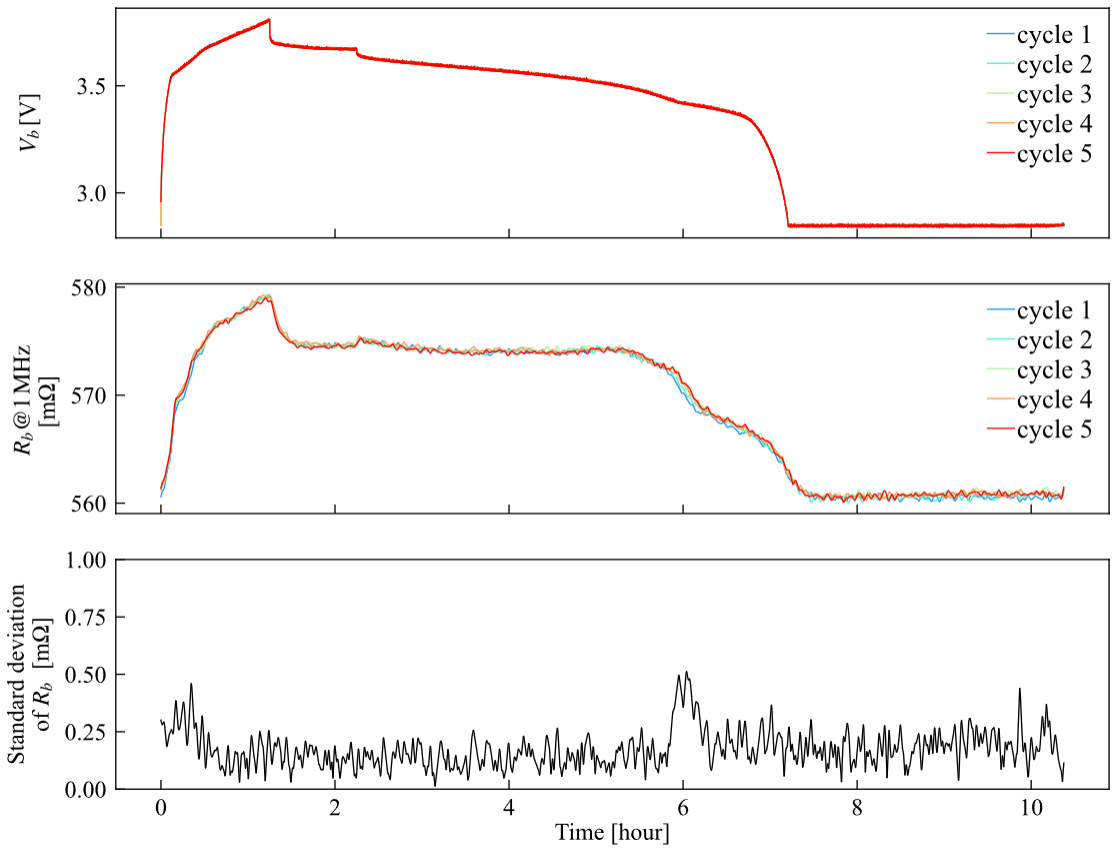

Figure S11. Measurement reproducibility and standard deviation of the sensor during 0.4C charge and 0.1C discharge cycles.

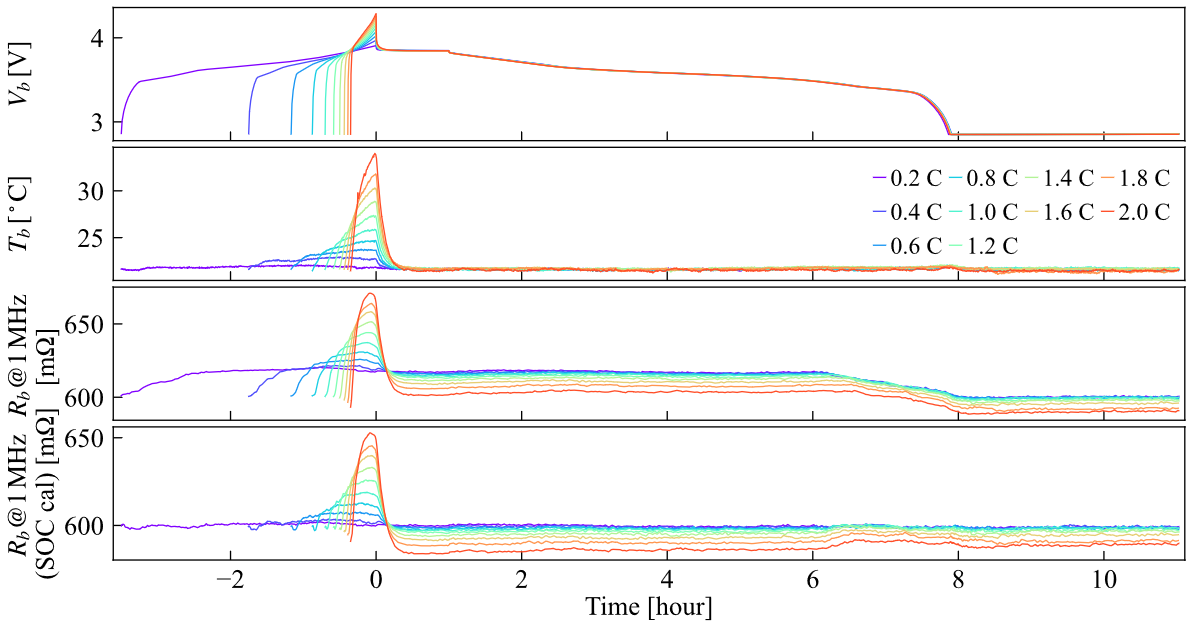

Figure S12. Stepwise C-rate test in which the charge rate was raised by 0.2 C each cycle, with each cycle being charged from 0 to 70% SOC.